Current Applied Science and Technology e-ISSN: 2586-9396

Curr. Appl. Sci. Technol. 2026, Vol. 26 (No.2), e0264845

Research article

Optimization of Needleless Electrospinning for the Large-Scale Production of Photocatalytic Nanofibers

Dwi Sabda Budi Prasetya[1,4]*, Edy Supriyanto[2], Novita Andarini[2], I Dewa Putu Hermida[3], Wibawa[4] and Ahmad Kusumaatmaja[5]

[1]Mandalika University of Education, Indonesia
[2]Jember University, Indonesia
[3]Centre for Telecommunication Research-BRIN, Indonesia
[4]PGRI University of Yogyakarta, Indonesia
[5]Gadjah Mada University, Indonesia

Received: 27 September 2024, Revised: 17 March 2025, Accepted: 14 April 2025, Published: 8 July 2025

Abstract

This study was focused on optimizing a needleless electrospinning process for the large-scale production of PVA/TiO_2/chitosan nanofibers. Using a custom-designed mushroom-shaped spinneret, key parameters including solution viscosity, electric field strength, flow rate, and spinneret-to-collector distance—were systematically varied and optimized to enhance fiber production efficiency and uniformity. Three spinneret designs, multiple solution compositions, and electric field strengths were tested to determine optimal conditions. The resulting nanofibers were characterized using FTIR, SEM, XRD, and EDX, confirming the successful integration of TiO_2 and chitosan into the polymer matrix. The mushroom-shaped spinneret demonstrated the highest production efficiency, producing uniform nanofibers with an average diameter of 150 nm and a throughput of 300 mg/h. Mechanical testing indicated an improved tensile strength of 9.2 MPa, while photocatalytic evaluation showed 82% methylene blue degradation after 180 min of UV exposure, confirming their potential for environmental remediation. Compared to conventional single-needle electrospinning, the needleless electrospinning setup exhibited higher throughput, better fiber uniformity, and improved control over nanofiber properties, indicating its viability for industrial-scale applications. Future research should explore long-term stability, advanced material combinations, and further parameter refinements to enhance large-scale nanofiber production.

Keywords: needleless electrospinning; PVA/TiO_2/chitosan nanofibers; photocatalytic activity; biomedical applications; environmental remediation; large-scale production

*Corresponding author: E-mail: dwisabda68@gmail.com
https://doi.org/10.55003/cast.2025.264845

1. Introduction

Nanofibers have gained significant attention due to their high surface area-to-volume ratio, tunable porosity, and mechanical strength, making them highly suitable for applications in biomedicine and environmental remediation (Huang et al., 2003; Greiner & Wendorff, 2007). Among various fabrication methods, electrospinning has emerged as a versatile and efficient technique, enabling the production of ultrafine fibers with controlled morphology and functional properties (Teo & Ramakrishna, 2006). In biomedical applications, electrospun nanofibers have been explored for wound healing, drug delivery, and tissue engineering. For instance, polycaprolactone/chitosan composite fibers exhibit antibacterial properties and promote cellular proliferation, making them ideal for wound dressing applications (Bhattarai et al., 2005). Additionally, their high porosity of electrospun nanofibers enables controlled drug release, improving therapeutic outcomes (Teo & Ramakrishna, 2006). In tissue engineering, electrospun nanofibers function as scaffolds, providing structural support and enhancing cellular activity, thus facilitating tissue regeneration (Yu et al., 2009; Ye et al., 2019).

For environmental applications, electrospun nanofibers are widely used in filtration systems for air and water purification. Their high surface area and porosity enable the efficient capture of contaminants, improving environmental health and safety (Nasikhudin et al., 2017). However, challenges related to the long-term stability and scalability of electrospun nanofiber production persist, limiting its widespread adoption. Addressing these challenges requires further research on material selection, process optimization, and application-specific evaluations (Teo & Ramakrishna, 2006; Bhattarai et al., 2010; Mondal, 2017). Needleless electrospinning has emerged as a promising alternative to traditional single-needle electrospinning, significantly enhancing throughput and production efficiency. This method facilitates the formation of multiple fiber jets simultaneously, overcoming the low-yield limitation of conventional setups (Mondal, 2017; Partheniadis et al., 2020; Xiong et al., 2021). The parameters governing needleless electrospinning can be categorized into independent and dependent variables, which influence fiber morphology and production outcomes (Yalcinkaya et al., 2016). Moreover, the electric field distribution and spinneret design critically affect jet initiation and fiber uniformity (Zhou et al., 2010; Wang et al., 2012). Despite these advancements, research gaps remain in controlling nanofiber morphology and quality at an industrial scale. Specifically, the relationship between processing parameters such as solution viscosity, electric field strength, and spinneret-to-collector distance and the resulting nanofiber properties has yet to be fully elucidated (Jirsak & Petrik, 2012).

This study investigates the optimization of needleless electrospinning parameters, focusing on three main factors:

1. Spinneret design: Comparative analysis of cylindrical, serrated disk, and mushroom-shaped spinnerets were performed to determine their impact on fiber morphology and production efficiency.

2. Solution properties: Variations in polymer concentration, solvent ratios, and TiO_2 content were examined to enhance fiber formation and structural integrity.

3. Electric field strength: The influence of different voltages on fiber diameter and uniformity was explored.

To evaluate production efficiency, fiber yield per unit time was measured, while nanofiber quality was assessed based on fiber uniformity, mechanical stability, and photocatalytic activity.

The ultimate goal of this study is to enhance the scalability of nanofiber production while ensuring high-quality fiber properties for industrial applications in environmental remediation and biomedicine. By systematically optimizing needleless electrospinning parameters, this work seeks to establish a scalable and efficient production pathway for functional nanofibers, offering significant advancements in large-scale nanofiber fabrication.

2. Materials and Methods

2.1 Chemicals and materials

The primary materials used in this study were polyvinyl alcohol (PVA), titanium dioxide (TiO_2) nanoparticles, and chitosan. PVA (98-99% hydrolyzed) was sourced from Sigma-Aldrich, while TiO_2 nanoparticles (<25 nm, anatase phase) were obtained from Alfa Aesar. Chitosan, with a deacetylation degree of ≥75%, was procured from Sigma-Aldrich. All chemicals were of analytical grade and used without further purification, selected for their proven efficacy in forming composite nanofibers for water treatment and biomedical applications (Bhattarai et al., 2010; Nasikhudin et al., 2017; Partheniadis et al., 2020).

2.2 Solution preparation

The electrospinning solutions were prepared by dissolving PVA in distilled water to achieve a 10 wt% solution and stirred at 90°C for 4 h until fully dissolved (Figure 1). Separately, TiO_2 nanoparticles (5 wt%) were dispersed into the PVA solution through ultrasonication for 30 min to ensure uniform distribution. Chitosan was dissolved in a 1% acetic acid solution to form a 2 wt% solution and combined with the PVA/TiO_2 mixture in a 1:1 ratio under constant stirring. The resulting homogeneous solution was used in the electrospinning process, designed to produce nanofibers with enhanced mechanical strength and photocatalytic activity (Bhattarai et al., 2005; Teo & Ramakrishna, 2006). The mechanical strength of the prepared nanofibers was confirmed through tensile strength testing using a Universal Testing Machine (UTM), while their photocatalytic activity was evaluated by measuring the degradation rate of methylene blue under UV irradiation. These tests provided quantitative validation of the nanofibers' structural integrity and functional performance (Yu et al., 2009; Jirsak & Petrik, 2012).

2.3 Needleless electrospinning setup and process

Needleless electrospinning setup with key components is shown in Figure 2. The processes are as follows:

Voltage power supply: A high-voltage power supply (15 kV) was used to generate the strong electric field necessary for electrospinning. This high voltage facilitated the formation of multiple jets from the free liquid surface of the spinning solution, a crucial factor in needleless electrospinning (Mondal, 2017; Partheniadis et al., 2020).

Solution reservoir and delivery system: The spinning solution was stored in a container designed with a mushroom-shaped spinneret at the top. A peristaltic pump controlled the flow rate of the solution to the spinneret, ensuring a steady and consistent supply of the polymer mixture. The delivery system was insulated to prevent electrical interference and ensure a stable electrospinning process (Yu et al., 2009; Yalcinkaya et al., 2016).

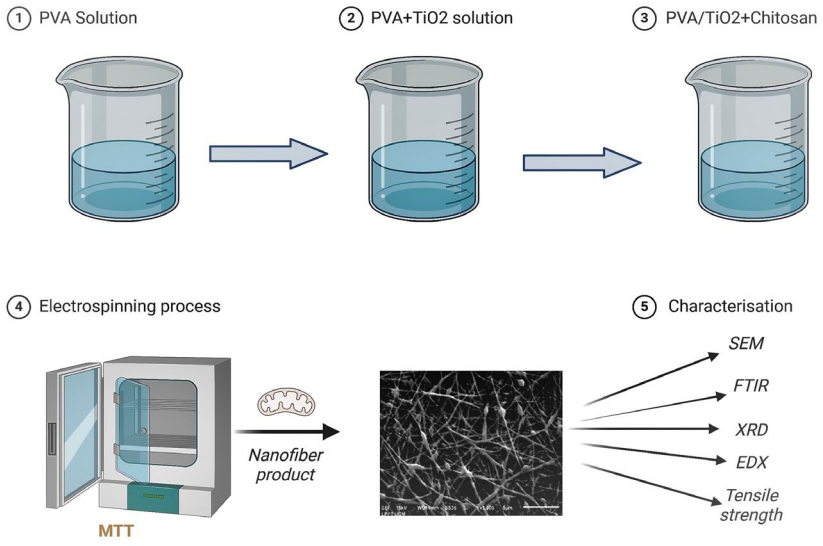

Figure 1. Schematic of the nanofiber fabrication process: (1) PVA solution preparation, (2) TiO_2 nanoparticle addition, (3) Chitosan incorporation, (4) Electrospinning, and (5) Characterization (SEM, FTIR, XRD, EDX, tensile testing)

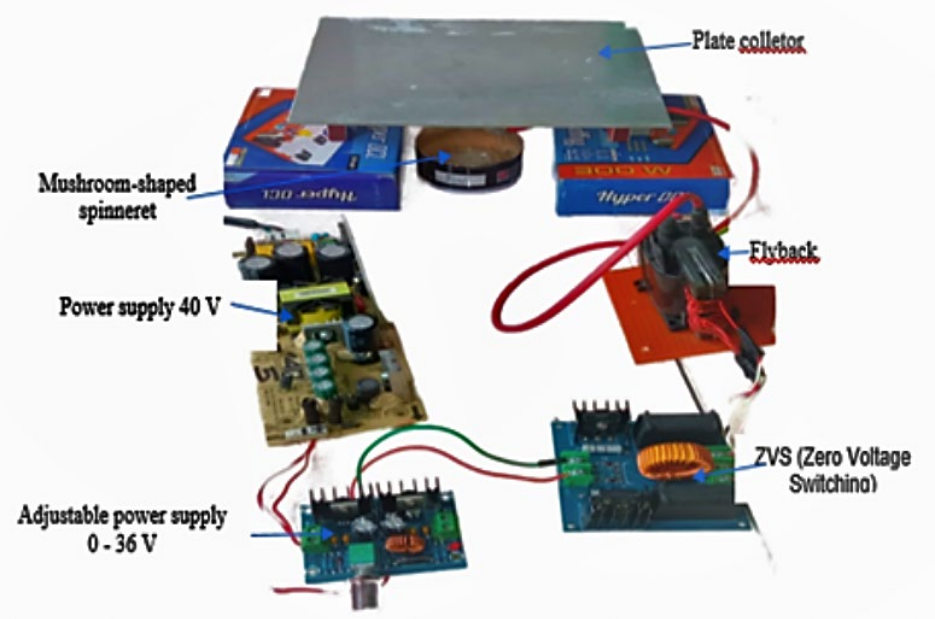

Figure 2. Needleless electrospinning setup with key components: voltage power supply, solution reservoir, mushroom-shaped spinneret, and collector

Mushroom-shaped spinneret: The central component of the needleless electrospinning setup was the mushroom-shaped spinneret, which was constructed from a metal base to enhance electrical conductivity. This spinneret was designed to facilitate the formation of stable pre-Taylor cones on its surface when exposed to the high-voltage electric field. The curved surface of the mushroom-shaped spinneret allowed for the generation of multiple jets, significantly increasing fiber production rates compared to traditional single-needle setups (Wang et al., 2012; Mondal, 2017; Xiong et al., 2021).

Collector: A flat plate collector was positioned below the spinneret to collect the electrospun fibers. The distance between the spinneret and the collector was optimized to ensure proper fiber formation and minimize defects. The grounded collector provided an electric field pathway, attracting the charged fibers and allowing them to deposit uniformly onto the collector surface (Yu et al., 2009; Zhou et al., 2010).

Electrospinning process: During operation, the PVA/TiO_2/chitosan solution was pumped onto the mushroom-shaped spinneret. Upon applying the high voltage of 15 kV, multiple jets were formed from the spinneret's surface, creating fine fibers that were drawn towards the collector by the electric field. The use of a mushroom-shaped spinneret allowed for the simultaneous formation of multiple jets, enhancing the throughput and production efficiency of the needleless electrospinning process (Xiong et al., 2021).

By optimizing each component and the process parameters (such as voltage, solution flow rate, and spinneret-to-collector distance), this setup successfully produced uniform and high-quality nanofibers suitable for large-scale applications in environmental remediation and biomedicine (Jirsak & Petrik, 2012; Yalcinkaya et al., 2016).

2.4 Characterization techniques

The morphological and structural characteristics of the electrospun nanofibers were analyzed using several techniques:

Scanning electron microscopy (SEM): Morphological analysis was performed using a Hitachi SU8010 microscope. Fiber diameters were measured using ImageJ software, with at least 100 fibers measured per sample to ensure statistical accuracy (Teo & Ramakrishna, 2006; Partheniadis et al., 2020).

Fourier transform infrared spectroscopy (FTIR): FTIR spectra were recorded on a Bruker Tensor 27 Spectrometer over the range of 4000-400 cm^{-1} to identify functional groups and confirm the incorporation of TiO_2 and chitosan into the PVA matrix (Yalcinkaya et al., 2016; Nasikhudin et al., 2017).

X-ray diffraction (XRD): XRD analysis was conducted using a Bruker D8 Advance diffractometer with Cu Kα radiation (λ = 1.5406 Å) over a 2θ range of 10°-80°. This analysis focused on determining the crystalline phases of TiO_2 and the interaction between PVA and chitosan within the nanofibers (Huang et al., 2003; Partheniadis et al., 2020).

Energy-dispersive X-ray spectroscopy (EDX): EDX analysis was performed to confirm the elemental composition and dispersion of TiO_2 nanoparticles within the nanofibers. The uniform distribution of TiO_2 was validated through EDX mapping (Yu et al., 2009; Partheniadis et al., 2020).

Tensile testing: Mechanical properties of the nanofibers were evaluated using a Universal Testing Machine (UTM), which measured tensile strength and elongation at break (Bhattarai et al., 2010; Jirsak & Petrik, 2012).

Photocatalytic activity assessment: The photocatalytic efficiency of the nanofibers was examined through methylene blue degradation under UV irradiation, measured using

a UV-Vis spectrophotometer. The degradation rate was used as an indicator of the photocatalytic performance of TiO_2-containing nanofibers (Teo & Ramakrishna, 2006).

This comprehensive characterization confirmed the structural integrity, chemical composition, and functional performance of the optimized PVA/TiO_2/chitosan nanofibers, validating their suitability for scalable industrial applications.

3. Results and Discussion

3.1 Optimization of spinneret design

Three different spinneret designs, cylindrical, serrated disk, and mushroom-shaped—were tested to evaluate their effect on nanofiber morphology and production efficiency. The mushroom-shaped spinneret exhibited the best performance, producing uniform fibers (~150 nm in diameter) with the highest production rate (300 mg/h) and minimal bead defects, as summarized in Table 1 (Mondal, 2017; Partheniadis et al., 2020).

Table 1. Comparison of different spinneret designs based on fiber diameter, production rate, and bead formation

Spinneret Design	Average Fiber Diameter (nm)	Production Rate (mg/h)	Bead Defects
Cylindrical	~200	180	High
Serrated Disk	~180	220	Moderate
Mushroom-shaped	~150	300	Low

The mushroom-shaped spinneret facilitated multiple stable jet formations, leading to an increase in production rate and fiber uniformity (Wang et al., 2009; Yalcinkaya et al., 2016; Mondal, 2017; Latiffah et al., 2022). SEM analysis confirmed that nanofibers produced with this spinneret were smooth and uniform, with fewer beads and structural defects.

3.2 Optimization of solution

Different PVA concentrations (8 wt%, 10 wt%, and 12 wt%), TiO_2 contents (3 wt%, 5 wt%, and 7 wt%), and chitosan concentrations (1 wt%, 2 wt%, and 3 wt%) were tested to optimize fiber formation. The best-performing solution contained 10 wt% PVA, 5 wt% TiO_2, and 2 wt% chitosan, resulting in improved fiber uniformity, mechanical strength (9.2 MPa), and photocatalytic efficiency (82%), as shown in Table 2.

Higher TiO_2 concentrations (>5 wt%) led to nanoparticle agglomeration, reducing fiber uniformity (Nasikhudin et al., 2017). Meanwhile, chitosan at 2 wt% enhanced the mechanical strength without compromising fiber integrity (Teo & Ramakrishna, 2006).

Table 2. Effect of solution composition on the mechanical strength and photocatalytic activity of electrospun PVA/TiO_2/chitosan nanofibers

Solution Composition	Tensile Strength (MPa)	Methylene Blue Degradation (%)
8 wt% PVA, 3 wt% TiO_2, 1 wt% chitosan	7.5	70
10 wt% PVA, 5 wt% TiO_2, 2 wt% chitosan	9.2	82
12 wt% PVA, 7 wt% TiO_2, 3 wt% chitosan	8.0	78

3.3 Optimization of electric field strength

Electric field strength plays a crucial role in fiber formation. Voltages between 10 kV and 20 kV were tested, and 15 kV was found to be optimal, producing the most uniform fibers (~150 nm) with the highest production rate (300 mg/h). Voltages below 12 kV resulted in bead formation, while those above 18 kV caused unstable jet separation (Jirsak & Petrik, 2012; Yalcinkaya et al., 2016; Xiong et al., 2021). These results are summarized in Table 3.

Table 3. Effect of applied voltage on fiber diameter, production rate, and morphological uniformity of electrospun PVA/TiO_2/chitosan nanofibers

Voltage (kV)	Fiber Diameter (nm)	Production Rate (mg/h)	Morphological Uniformity
10	~220	150	Non-uniform
12	~180	200	Moderate
15	~150	300	Uniform
18	~170	250	Less stable
20	~190	220	Unstable

3.4 Characterization of nanofibers

3.4.1 FTIR analysis

Fourier transform infrared (FTIR) spectroscopy confirmed the successful integration of PVA, chitosan, and TiO_2 within the nanofiber matrix. The FTIR spectrum exhibited characteristic peaks at 3379 cm^{-1} (O–H and N–H stretching), 1655 cm^{-1} (amide I band from chitosan), 1095 cm^{-1} (C–O stretching of PVA), and 550 cm^{-1} (Ti–O stretching of TiO_2). The minor shift in the O–H stretching peak compared to pure PVA indicated hydrogen bonding interactions between PVA, chitosan, and TiO_2, ensuring uniform dispersion (Nasikhudin et al., 2017). In Figure 3, the broad peak around ~3379 cm^{-1} corresponds to O–H and N–H stretching vibrations, indicating the presence of hydroxyl groups from PVA and amino groups from chitosan. The peak near ~2925 cm^{-1} is attributed to C–H stretching in the PVA backbone. A distinct band at ~1655 cm^{-1} corresponds to the amide I group,

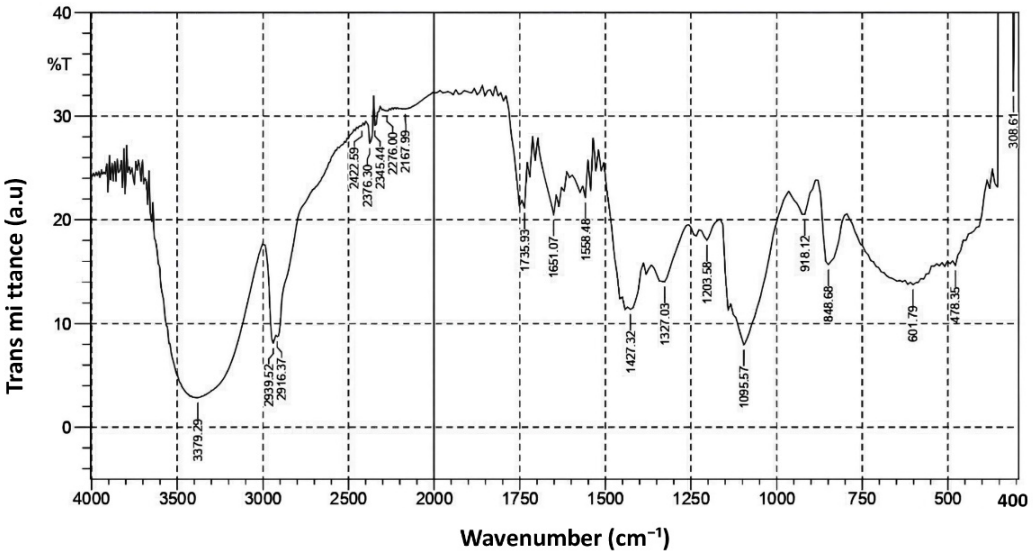

Figure 3. FTIR spectrum of electrospun PVA/TiO_2/chitosan nanofibers

confirming chitosan incorporation. The ~1095 cm^{-1} peak represents C–O stretching vibrations from PVA, while the peak near ~550 cm^{-1} is assigned to Ti–O stretching, confirming the presence of TiO_2 nanoparticles. These characteristic peaks validate the successful integration of TiO_2 and chitosan within the PVA nanofiber matrix.

3.4.2 EDX analysis

Energy dispersive X-ray spectroscopy (EDX) confirmed the presence of titanium (Ti), oxygen (O), and carbon (C), validating the incorporation of TiO_2 nanoparticles into the nanofiber structure. Additionally, EDX mapping showed a uniform dispersion of TiO_2, which is crucial for maintaining consistent photocatalytic activity (Yu et al., 2009; Nasikhudin et al., 2017; Partheniadis et al., 2020). In Figure 4, the spectrum confirms the presence of carbon (C), oxygen (O), and titanium (Ti), which are associated with the PVA/chitosan polymer matrix and the TiO_2 nanoparticles. The clear Ti peaks verify the successful incorporation of TiO_2 into the nanofiber structure. Minor signals for sodium (Na) and aluminum (Al) were also detected, likely originating from the substrate or residual impurities. Overall, the elemental composition supports the expected chemical structure of the composite nanofibers.

3.4.3 SEM analysis

Scanning electron microscopy (SEM) images revealed that the electrospun nanofibers had a smooth and uniform morphology, with an average fiber diameter of ~150 nm. The absence of bead formation confirmed that optimized parameters led to stable jet formation and controlled fiber deposition (Xiong et al., 2021). Figure 5 shows an SEM image of electrospun PVA/TiO_2/chitosan nanofibers at 15 kV and 5000× magnification. The fibers exhibited a uniform, interconnected structure with some bead formation, indicating the influence of solution parameters and electrospinning conditions on fiber morphology.

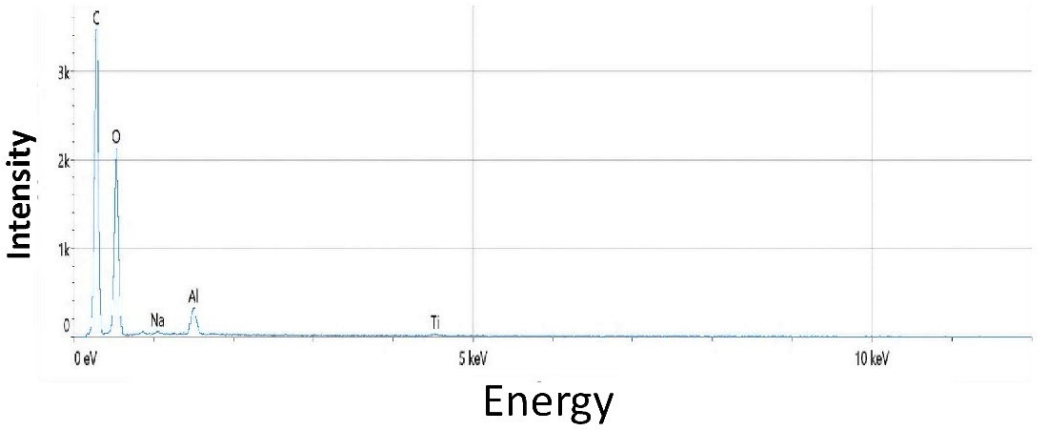

Figure 4. EDX spectrum of electrospun PVA/TiO_2/chitosan nanofibers, confirming the presence of key elements: carbon (C), oxygen (O), titanium (Ti), sodium (Na), and aluminum (Al)

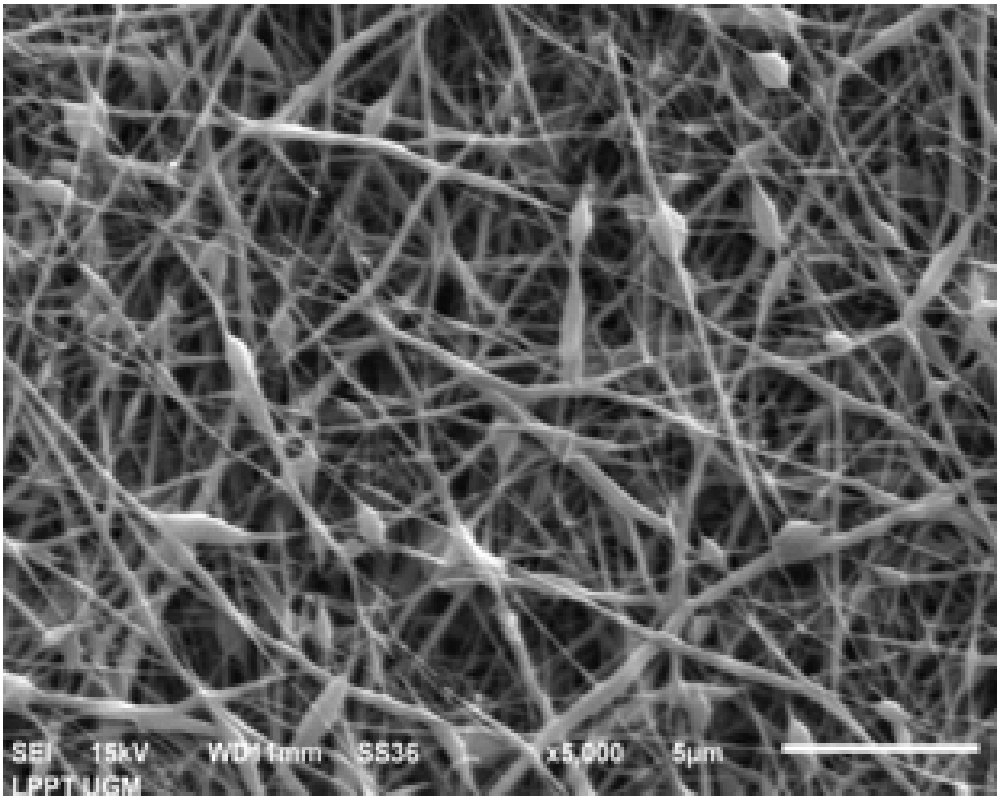

Figure 5. SEM image of nanofibers showing uniform morphology with minimal bead formation

3.4.4 XRD analysis

Figure 6 shows X-ray diffraction (XRD) analysis with identification of distinct peaks at 2θ = 25.3°, 37.8°, 48.0°, and 54.0°, corresponding to the (101), (004), (200), and (105) planes of anatase-phase TiO_2, respectively. The presence of anatase-phase TiO_2 is significant, as it is known for its high photocatalytic activity under UV light (Huang et al., 2003; Nasikhudin et al., 2017; Partheniadis et al., 2020).

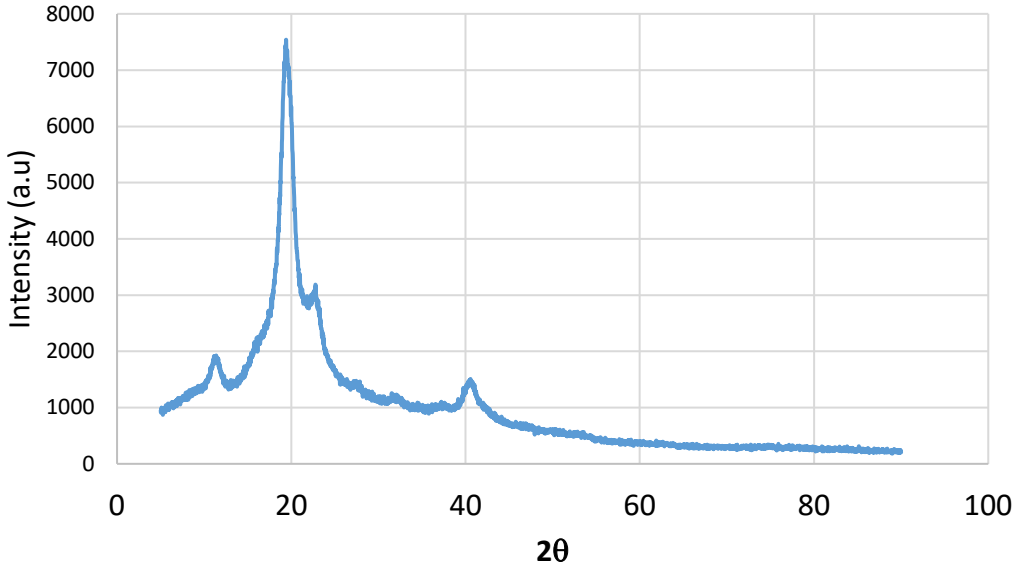

Figure 6. XRD pattern of electrospun PVA/TiO_2/chitosan nanofibers, showing anatase-phase TiO_2 (101) at ~25.3°

3.4.5 Mechanical stability

Tensile testing indicated that the incorporation of 2 wt% chitosan improved the mechanical strength of nanofibers, achieving a tensile strength of 9.2 MPa (Table 4). This enhancement was attributed to intermolecular interactions between PVA and chitosan, which reinforced the polymer matrix (Teo & Ramakrishna, 2006).

3.4.6 Photocatalytic activity

The photocatalytic performance of the nanofibers was assessed by measuring the degradation rate of methylene blue (MB) under UV irradiation (Table 5). The TiO_2-containing nanofibers exhibited an 82% degradation efficiency after 180 min of UV exposure, significantly higher than that of PVA/chitosan fibers without TiO_2. This confirms the role of anatase-phase TiO_2 in enhancing photocatalytic activity, making the nanofibers suitable for environmental applications (Yu et al., 2009, Nasikhudin et al., 2017; Ye et al., 2019; Partheniadis et al., 2020).

Table 4. Effect of chitosan content on the tensile strength of electrospun PVA/TiO_2/chitosan nanofibers

Sample Composition	Chitosan Content (wt%)	Tensile Strength (MPa)	Improvement Description
PVA/TiO_2 (without chitosan)	0	7.5	Baseline sample
PVA/TiO_2/Chitosan	1	8.2	Slight improvement
PVA/TiO_2/Chitosan	2	9.2	Optimal reinforcement
PVA/TiO_2/Chitosan	3	8.5	Excess chitosan reduced fiber strength

Table 5. Effect of TiO_2 content on the photocatalytic degradation of methylene blue under UV irradiation

Sample Composition	TiO_2 Content (wt%)	UV Exposure Time (min)	Methylene Blue Degradation (%)
PVA/Chitosan (without TiO_2)	0	180	35
PVA/Chitosan/TiO_2	3	180	70
PVA/Chitosan/TiO_2	5	180	82
PVA/Chitosan/TiO_2	7	180	78

3.5 Summary of findings

The optimized needleless electrospinning process successfully produced uniform PVA/TiO_2/chitosan nanofibers with enhanced mechanical strength and photocatalytic properties. The key findings include:

- Mushroom-shaped spinneret enabled the highest throughput and best fiber uniformity.
- Optimal solution composition (10 wt% PVA, 5 wt% TiO_2, and 2 wt% chitosan) provided superior mechanical and photocatalytic properties.
- Optimal applied voltage (15 kV) ensured stable jet formation and uniform fiber deposition.
- Nanofibers demonstrated superior mechanical strength (9.2 MPa) and high photocatalytic activity (82% degradation efficiency).

These results indicate that the developed nanofibers hold significant potential for scalable production in biomedical and environmental sectors (Jirsak & Petrik, 2012; Yalcinkaya et al., 2016; Partheniadis et al., 2020). Table 4 and Table 5 provide further detailed results on the mechanical strength and photocatalytic degradation efficiency (Teo & Ramakrishna, 2006; Yu et al., 2009; Ye et al., 2019; Nasikhudin et al., 2017).

4. Conclusions

This study successfully optimized needleless electrospinning for the large-scale production of PVA/TiO_2/chitosan nanofibers, achieving high fiber uniformity, improved mechanical strength, and enhanced photocatalytic activity. The mushroom-shaped spinneret yielded the best fiber morphology (~150 nm) and highest production rate (300 mg/h). The optimal solution composition (10 wt% PVA, 5 wt% TiO_2, 2 wt% chitosan) resulted in 9.2 MPa tensile strength and 82% methylene blue degradation efficiency. Applying 15 kV voltage ensured stable jet formation and uniform fiber deposition.

Characterization confirmed successful material integration (FTIR, EDX), uniform fiber structure (SEM), anatase-phase TiO_2 for photocatalysis (XRD), and strong mechanical properties (tensile testing). These findings demonstrate the scalability of needleless electrospinning for biomedical and environmental applications.

Future research should focus on long-term stability of nanofibers under real-world conditions, exploration of other material combinations for enhanced functionality and industrial-scale automation to increase production efficiency and reduce costs. This study shows that needleless electrospinning offers a promising pathway for large-scale nanofiber production with applications in environmental remediation and biomedicine, paving the way for future advancements in nanomaterial manufacturing.

5. Acknowledgements

We would like to express our deepest gratitude to the National Research and Innovation Agency (BRIN), Education Fund Management Organization (LPDP) the Ministry of Finance of the Republic of Indonesia, as well as the Material Physics and Instrumentation Laboratory FMIPA UGM, and various parties who helped and supported us.

6. Authors' Contributions

Dwi Sabda Budi Prasetya: Wrote the manuscript, designed the experiments, and analyzed the results. Edy Supriyanto: Developed the research concept and supported the manuscript writing. Novita Andarini: Conducted experiments, collected data, and performed characterization analysis. I Dewa Putu Hermida: Assisted in data analysis and interpretation of results. Wibawa: Contributed to the experimental design and process optimization. Ahmad Kusumaatmaja: As the main supervisor, provided technical guidance in experiments and data analysis, and assisted in the manuscript preparation.

7. Conflicts of Interest

The authors declare that there is no conflict of interest regarding the publication of this article. The authors also confirm that the paper is free of plagiarism.

References

Bhattarai, N., Gunn, J., & Zhang, M. (2010). Chitosan-based hydrogels for controlled, localized drug delivery. *Advanced Drug Delivery Reviews*, 62(1), 83-99. https://doi.org/10.1016/j.addr.2009.07.019

Greiner, A., & Wendorff, J. H. (2007). Electrospinning: A fascinating method for the preparation of ultrathin fibers. *Angewandte Chemie International Edition,* 46(30), 5670-5703. https://doi.org/10.1002/anie.200604646

Huang, Z.-M., Zhang, Y.-Z., Kotaki, M., & Ramakrishna, S. (2003). A review on polymer nanofibers by electrospinning and their applications in nanocomposites. *Composites Science and Technology,* 63(15), 2223-2253. https://doi.org/10.1016/S0266-3538(03)00178-7

Jirsak, O., & Petrik, S. (2012). Recent advances in nanofibre technology: needleless electrospinning. *International Journal of Nanotechnology*, 9(8-9), 836-845. https://doi.org/10.1504/IJNT.2012.046756

Latiffah, E., Agung, B. H., Hapidin, D. A., & Khairurrijal, K. (2022). Fabrication of polyvinylpyrrolidone (PVP) nanofibrous membranes using mushroom-spinneret needleless electrospinning. *Journal of Physics: Conference Series*, 2243, Article 012101. https://doi.org/10.1088/1742-6596/2243/1/012101

Mondal, K. (2017). Recent advances in the synthesis of metal oxide nanofibers and their environmental remediation applications. *Inventions*, *2*(2), Article 9. https://doi.org/10.3390/inventions2020009

Nasikhudin, Ismaya, E. P., Diantoro, M., Kusumaatmaja, A., & Triyana, K. (2017). Preparation of PVA/TiO2 composites nanofibers by using electrospinning method for photocatalytic degradation. *IOP Conference Series: Materials Science and Engineering*, 202(1), Article 012011. https://doi.org/10.1088/1757-899X/202/1/012011

Partheniadis, I., Nikolakakis, I., Laidmäe, I., & Heinämäki, J. (2020). A mini-review: Needleless electrospinning of nanofibers for pharmaceutical and biomedical applications. *Processes*, 8(6), Article 673. https://doi.org/10.3390/pr8060673

Teo, W. E., & Ramakrishna, S. (2006). A review on electrospinning design and nanofiber. *Nanotechnology,* 17(14), R89-R106. https://doi.org/10.1088/0957-4484/17/14/R01

Wang, X., Niu, H., Lin, T., & Wang, X. (2009). Needleless electrospinning of nanofibers with a conical wire coil. *Polymer Engineering and Science*, 49, 1582-1586. https://doi.org/10.1002/pen.21377

Wang, X., Wang, X., & Lin, T. (2012). Electric field analysis of spinneret design for needleless electrospinning of nanofibers. *Journal of Materials Research*, 27(23), 3013-3019. https://doi.org/10.1557/jmr.2012.346

Xiong, J., Liu, Y., Li, A., Wei, L., Wang, L., Qin, X., & Yu, J. (2021). Mass production of high-quality nanofibers via constructing pre-Taylor cones with high curvature on needleless electrospinning. *Materials and Design*, 197, Article 109247. https://doi.org/10.1016/j.matdes.2020.109247

Yalcinkaya, F., Yalcinkaya, B., & Jirsak, O. (2016). Dependent and independent parameters of needleless electrospinning. In S. Haider, & A. Haider (Eds.). *Electrospinning - Material techniques, and biomedical applications* (pp. 67-93). IntechOpen. https://doi.org/10.5772/65838

Ye, K., Kuang, H., You, Z., Morsi, Y., & Mo, X. (2019). Electrospun nanofibers for tissue engineering with drug loading and release. *Pharmaceutics*, 11(4), Article 182. https://doi.org/10.3390/pharmaceutics11040182

Yu, D.-G., Zhu, L.-M., White, K., & Branford-White, C. (2009). Electrospun nanofiber-based drug delivery systems. *Health*, 1(2), 67-75. https://doi.org/10.4236/health.2009.12012

Zhou, F.-L., Gong, R.-H., & Porat, I. (2010). Needle and needleless electrospinning for nanofibers. *Journal of Applied Polymer Science*, 115(5), 2591-2598. https://doi.org/10.1002/app.31282